Optimal $\mathcal{H}_2$ and $\mathcal{H}_\infty$ Control of Extremely Large Segmented Telescopes

Zaher M. Kassas*
The University of Texas at Austin, Austin, TX, 78712, USA
Robert H. Bishop†
Marquette University, Milwaukee, WI, 53233, USA

Extremely large telescopes (ELTs) are the next generation of ground-based reflecting telescopes of optical wavelengths. ELTs possess an aperture of more than 20 meters and share a number of common features, particularly the use of a segmented primary mirror and adaptive optics systems. In 2005, the European Southern Observatory introduced a new giant telescope concept, named the European Extremely Large Telescope (E-ELT), which is scheduled for operation in 2018. In 2009, a feasibility study proved the feasibility of the real-time (RT) control system architecture for the E-ELT's primary mirror, which consists of nearly 1,000 mirror segments with 3,000 actuators and 6,000 sensors. The goal of the RT control system was to maintain a perfectly aligned field of mirrors at all times with a loop-time of 1 ms. The study assumed a prescribed controller algorithm. This paper prescribes two such controllers. In this respect, optimal controller designs for the primary mirror, where optimality is formulated in the $\mathcal{H}_2$ and $\mathcal{H}_\infty$ frameworks are derived. Moreover, the designed controllers are simulated to show that the desired performance, which is defined in terms of imaging requirements, is met.

I. Introduction

Modern astronomical research requires investigating extremely faint objects that have small angular diameters. Large aperture telescopes provide higher spatial and spectral resolution that enables the detection of the astronomical objects in question. Early hints about how stars and galaxies formed are being discovered with the deployment of large ground and space telescopes. By pushing the capabilities of ground telescopes to their limits using extremely large telescopes (ELTs), astronomers are hoping to answer several lingering questions about our universe.

At the present time, the world's largest telescope is the Keck telescope. The Keck's primary mirror is 10 meters (m) in diameter. It consists of 36 hexagonal segments, which are adjusted twice per minute to compensate for gravity and other environmental effects as the telescope moves.[1]

In the 1990s, a consortium of universities proposed the first of the next generation of ELTs, the California Extremely Large Telescope (CELT), which was renamed the Thirty Meter Telescope (TMT).[2] The design of the TMT has a 30 m segmented primary mirror consisting of 492 segments with the out-of-plane degrees of freedom (DOF) actively controlled. Three precise position actuators, placed behind each segment, maintain the segment in-phase with its neighbors to a small fraction of light wavelength. Also, the TMT has a 3 m secondary mirror requiring 5 DOF control.[3]

Since 2005, the European Southern Observatory (ESO) has been defining a new ELT named the European Extremely Large Telescope (E-ELT).[4] The E-ELT will address key scientific challenges and will aim for

*Graduate Research Assistant, Department of Electrical & Computer Engineering, The University of Texas at Austin, zkassas@ieee.org
†Dean of the College of Engineering, Marquette University, robert.bishop@marquette.edu

a number of notable firsts, including discovering Earth-like planets around other stars in the "habitable zones" where life could exist. Other answers the E-ELT will attempt to uncover include understanding the relationship between black holes and galaxies, measuring the properties of the first stars and galaxies, and probing the nature of dark matter and dark energy. An artist's depiction of the E-ELT is illustrated in Figure 1.

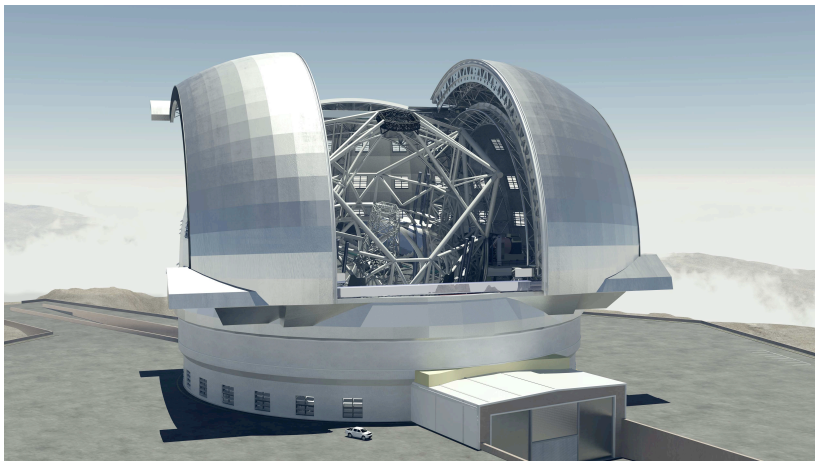

Figure 1. Artist depiction of the E-ELT.

The E-ELT primary segmented mirror, denoted as $M1$, consists of 984 hexagonal mirrors each weighing nearly 150 kg with diameters of 1.4 m for a total 42 m in diameter. In comparison, the diameter of the primary mirror of the Hubble Space Telescope is 2.4 m. In the $M1$ operation, adjacent mirror segments may tilt with respect to each other. This deviation is monitored using edge sensors. Actuator legs can move the segment 3 degrees in any direction. The 984 mirror segments comprise a system of 3,000 actuators and 6,000 sensors. Controlling the system of mirrors requires a vast amount of processing capability.

Since the control system design can impact the construction characteristics of the telescope, it is critical to assess the feasibility of the proposed control system architecture. For this purpose, a two-step study is conducted. The first study is to build a real-time (RT) simulation of the $M1$ mirror to perform hardware-in-the-loop (HIL) testing. The goal is to maintain a perfectly aligned field of mirrors at all times with a loop-time of 1 ms. For the purposes of HIL testing, the controller algorithm was assumed to be prescribed. Consequently, a case study was conducted to verify the feasibility of the control system architecture using LabVIEW deployed to a multi-core PC running LabVIEW RT Module.[5] The architecture incorporated two Dell Workstations, each with eight cores and a notebook that provided an operator interface. One Workstation simulated the telescope, whereas the other Workstation simulated the controller algorithm. The HIL $M1$ simulator is depicted in Figure 2. The required computational power was provided by multi-core implementations and supplemented by graphical processing units (GPUs) and field-programmable gate arrays (FPGAs). The study concluded that within the specified 1 ms loop-time, it is feasible to obtain the sensor data, send the data to the controller, compute the control signal, and send the control signal to the actuators.[6]

The second study is the topic of this paper, where we focus on prescribing optimal controller designs with a desired performance defined in terms of imaging requirements. In this respect, optimal controller designs for $M1$, where optimality is formulated in the $\mathcal{H}_2$ and $\mathcal{H}_\infty$ frameworks are derived. Moreover, the closed-loop system comprised of the designed controllers, telescope dynamics, and exogenous disturbances, is simulated.

This paper is organized as follows. Section II discusses the optical design of the E-ELT and models the $M1$ mirror. Sections III and IV formulate the $\mathcal{H}_2$ and $\mathcal{H}_\infty$ control design problems, respectively. Section V presents open- and closed-loop simulations of the overall system. Concluding remarks and future work are discussed in Section VI.

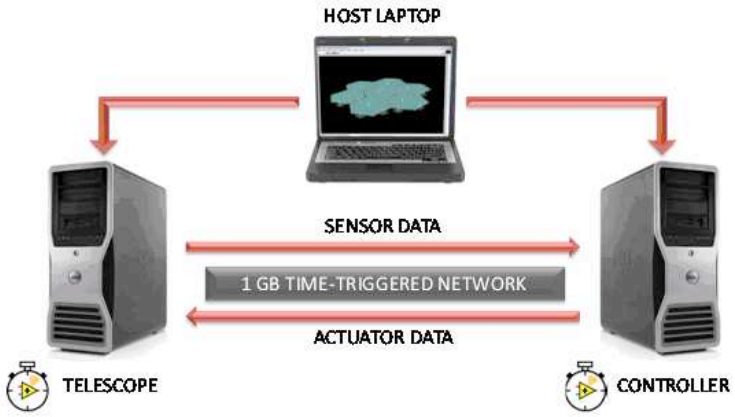

Figure 2. Hardware-in-the-loop $M1$ simulator

II. System Modeling

A. Optical design

The concept for the E-ELT is a telescope whose primary mirror is 42 m in diameter covering a field on the sky about a tenth the size of the full Moon. The optical design, depicted in Figure 3, is based on a five-mirror scheme that results in an exceptional image quality. The primary mirror consists of 984 segments, each 1.4 m wide, but only 50 mm thick. The E-ELT control system includes control loops for positioning the primary and secondary mirrors and control loops for adaptive optics. The crucial factor that determines the imaging quality is the performance of the primary mirror control system, which is the topic of this paper.

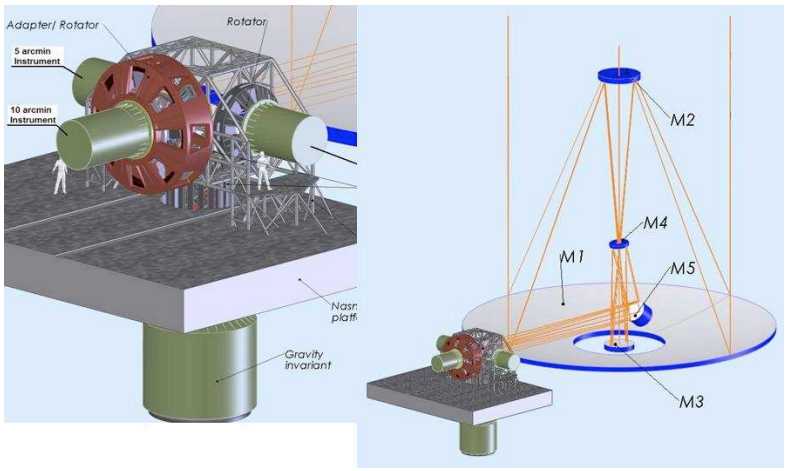

Figure 3. E-ELT optical system

B. Structure of the primary mirror system

On the back of each $M1$ mirror segment, 3 displacement actuators are installed to provide 3 out-of-plane DOF: piston, tip, and tilt. Moreover, each segment is equipped with 6 precision capacitive edge sensors that measure the relative surface displacements between adjacent segments. The optimal choice of the segment size is a function of several factors. Smaller segments are easier to support against gravity, easier to handle, and allow fewer optical surfaces to be used. However, smaller segments require more actuators and edge sensors besides other disadvantages.[7]

In this paper, we formulate and solve the $\mathcal{H}_2$ and $\mathcal{H}_\infty$ optimal control design problem of the seven-segment system illustrated in Figure 4. The control of the entire telescope becomes an extension of the seven-segment system to as many segments the telescope possesses.

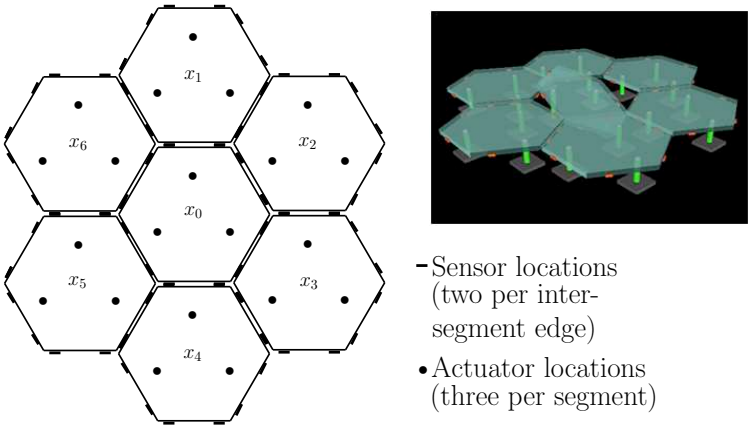

Figure 4. Seven-segment system

C. Dynamics of the primary mirror system

We adopt a nodal model to describe the dynamics of the mirror segments.[8] In particular, our model consists of localized masses mounted on springs and dampers and is governed by the differential equations

$$\mathbf{M}\ddot{\mathbf{q}} + \mathbf{D}\dot{\mathbf{q}} + \mathbf{J}\mathbf{q} = \mathbf{B_w}\mathbf{w} + \mathbf{B_u}\mathbf{u},$$

where $\mathbf{q} \in \mathbb{R}^{n_d}$, $\dot{\mathbf{q}} \in \mathbb{R}^{n_d}$, and $\ddot{\mathbf{q}} \in \mathbb{R}^{n_d}$ are the nodal displacements, velocities, and accelerations, respectively; $\mathbf{M} \in \mathbb{R}^{n_d \times n_d}$ is the mass matrix, $\mathbf{D} \in \mathbb{R}^{n_d \times n_d}$ is the damping matrix, $\mathbf{J} \in \mathbb{R}^{n_d \times n_d}$ is the stiffness matrix, $\mathbf{w} \in \mathbb{R}^{n_w}$ is the disturbance to the system, $\mathbf{u} \in \mathbb{R}^{n_u}$ is the control force, and n_d is the number of DOF the system has (3 in this case), n_w is the number of disturbances affecting the system, and n_u is the number control forces applied to the system. To simplify the modeling procedure, we assume that the supporting foundation is fixed and each segment is supported by three springs with damping.

We define the state vector of the i^{th} segment as $\mathbf{x}_i \triangleq \begin{bmatrix} \mathbf{q}_i^\mathsf{T} & \dot{\mathbf{q}}_i^\mathsf{T} \end{bmatrix}^\mathsf{T}$. Consequently, the nodal representation can be converted into the state-space representation

$$\dot{\mathbf{x}}_i = \mathbf{A}_i\mathbf{x}_i + \mathbf{B}_{1,i}\mathbf{w}_i + \mathbf{B}_{2,i}\mathbf{u}_i,$$

where

$$\mathbf{A}_i = \begin{bmatrix} \mathbf{0} & \mathbf{I} \\ -\mathbf{M}_i^{-1}\mathbf{J}_i & -\mathbf{M}_i^{-1}\mathbf{D}_i \end{bmatrix}, \quad \mathbf{B}_{1,i} = \begin{bmatrix} \mathbf{0} \\ -\mathbf{M}_i^{-1}\mathbf{B}_{w,i} \end{bmatrix}, \quad \mathbf{B}_{2,i} = \begin{bmatrix} \mathbf{0} \\ -\mathbf{M}_i^{-1}\mathbf{B}_{u,i} \end{bmatrix},$$

where $\mathbf{x}_i \in \mathbb{R}^6$ is the segment state vector, $\mathbf{w}_i$ denotes the disturbance inputs, and $\mathbf{u}_i$ denotes the control forces on the i^{th} segment. Finally, the dynamics of the complete system with $n+1$ segments is expressed as

$$\dot{\mathbf{x}} = \mathbf{A}\mathbf{x} + \mathbf{B}_1\mathbf{w} + \mathbf{B}_2\mathbf{u}, \tag{1}$$

where

$$\mathbf{A} = \operatorname{diag}\Big[\mathbf{A}_0 \ \cdots \ \mathbf{A}_n\Big], \ \mathbf{B}_i = \operatorname{diag}\Big[\mathbf{B}_{i,0} \ \cdots \ \mathbf{B}_{i,n}\Big], \ i \in \{1,2\}$$

$$\mathbf{x} = \Big[\mathbf{x}_0^\mathsf{T} \ \cdots \ \mathbf{x}_n^\mathsf{T}\Big]^\mathsf{T}, \ \mathbf{w} = \Big[\mathbf{w}_0^\mathsf{T} \ \cdots \ \mathbf{w}_n^\mathsf{T}\Big]^\mathsf{T}, \ \mathbf{u} = \Big[\mathbf{u}_0^\mathsf{T} \ \cdots \ \mathbf{u}_n^\mathsf{T}\Big]^\mathsf{T}.$$

D. Wind disturbance

The disturbances that affect the primary mirror system can be categorized into optical wavefront disturbances from the atmosphere and mechanical disturbances. The mechanical disturbance sources include gravity deformations, thermal variations, wind, and vibrations from drives and motors. Among these, wind disturbances are very significant to the operation of a large segmented telescope, and if we can reject these disturbances, the other sources can be readily addressed. For dynamic wind disturbances, we adopt the Von Karman model with the wind pressure power spectral density (PSD) given by

$$\Phi_{pt}^{\nu K}(f) = \frac{C_{pt}^{\nu K}}{\left[1 + (\frac{f}{f_0})^2\right]^{\frac{7}{6}}}.$$

We note that the PSD is fully defined by two parameters, the magnitude $C_{pt}^{\nu K}$ and the bandwidth f_0. For most wind disturbances, the bandwidth is 1 Hz,.[9] Based on empirical measured wind PSD, we can identify $C_{pt}^{\nu K} = 10$.[10] Moreover, based on least-squares estimate (LSE) method we can reconstruct the wind disturbance by passing white noise through a filter with transfer function (TF) $W_{wn}(s)$ and a corresponding state-space realization given as

$$\dot{\boldsymbol{\xi}}_i = \mathbf{A}_{\xi_i}\,\boldsymbol{\xi}_i + \mathbf{B}_{\xi_i}\,w_{0_i}, \quad w_i = \mathbf{C}_{\xi_i}\,\boldsymbol{\xi}_i,$$

where w_{0_i} is the input white noise to the reconstruction filter and w_i is the output of the filter. The Bode magnitude plot of such system is illustrated in Figure 5, which closely matches the measured PSD of wind disturbances.[8]

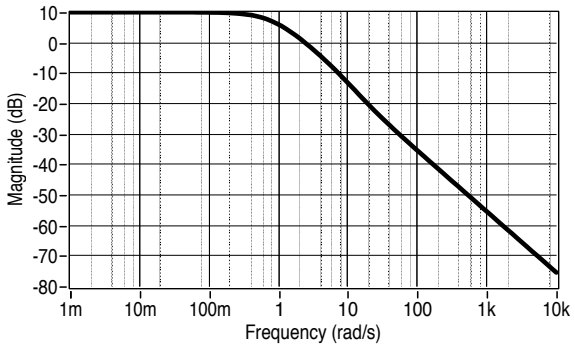

Figure 5. Bode magnitude plot of wind disturbance reconstruction filter

For simplicity, we assume that the wind disturbance is applied equally to the three supporting points; hence, the noise disturbance model affecting $n+1$ segments of the telescope is given by

$$\dot{\boldsymbol{\xi}} = \mathbf{A}_{\xi}\,\boldsymbol{\xi} + \mathbf{B}_{\xi}\,\mathbf{w}_0, \quad \mathbf{w} = \mathbf{C}_{\xi}\,\boldsymbol{\xi}, \tag{2}$$

$$\mathbf{A}_{\xi} = \text{diag}\Big[\mathbf{A}_{\xi_0}\ \cdots\ \mathbf{A}_{\xi_n}\Big],\ \mathbf{B}_{\xi} = \text{diag}\Big[\mathbf{B}_{\xi_0}\ \cdots\ \mathbf{B}_{\xi_n}\Big],\ \mathbf{C}_{\xi} = \text{diag}\Big[\mathbf{C}_{\xi_0}\ \cdots\ \mathbf{C}_{\xi_n}\Big]$$

$$\boldsymbol{\xi} = \Big[\boldsymbol{\xi}_0\ \cdots\ \boldsymbol{\xi}_n^{\mathsf{T}}\Big]^{\mathsf{T}},\ \mathbf{w}_0 = \Big[w_{0_0}^{\mathsf{T}}\ \cdots\ w_{0_n}^{\mathsf{T}}\Big]^{\mathsf{T}},\ \mathbf{w} = \Big[w_0^{\mathsf{T}}\ \cdots\ w_n^{\mathsf{T}}\Big]^{\mathsf{T}}.$$

E. Edge sensor model

Ideally, the relative displacements between the adjacent segments should be controlled to be less than one tenth of the operating wavelength. At this accuracy level, the best solution is to sense the position of each segment edge with respect to those of its neighbors. Typically, two edge sensors are required per edge to provide the relative height and twist of adjacent segments. For control design purposes, we will assume that

the outputs that become locally available from sensing at each segment, i, are the direct displacements of the three supporting points, i.e.

$$\mathbf{y}_i = \mathbf{C}_i \mathbf{x}_i, \quad \mathbf{C}_i = \begin{bmatrix} \mathbf{I}_{3\times 3} & \mathbf{0}_{3\times 3} \end{bmatrix},$$

where for simplicity, we assume that the measurement noise is negligible, which is motivated by the fact that it is of smaller magnitude as compared to the wind disturbance. Hence, if we can address the wind disturbance issue, adding the noise model of the sensors in the design process should be straightforward.

Combining the measurements for the $n+1$ segments, yields the measurement equation

$$\mathbf{y} = \mathbf{C}\mathbf{x}, \quad \mathbf{C} = \operatorname{diag}\begin{bmatrix} \mathbf{C}_0 & \cdots & \mathbf{C}_n \end{bmatrix}. \tag{3}$$

Numerical values for the system matrices are given in the Appendix.

F. Imaging performance requirements

For an optical system, the imaging performance is characterized by its point spread function, i.e. the light intensity distribution resulting from a point source. However, such function is two-dimensional and is very complex. For convenience, we adopt a commonly used practical criterion known as the Strehl ratio. The Strehl ratio is the ratio of the peak intensity in the actual image compared to the peak theoretical diffraction intensity. According to the Maréchal rule, an optical system is considered diffraction limited if the Strehl ratio is 0.8.[1] To maintain a Strehl ratio greater than 0.7, we have to control the relative displacements of the segments at the 0.1 μm order.[8]

III. Optimal $\mathcal{H}_2$ Controller Design for a Seven-Segment System

This section formulates the $\mathcal{H}_2$ optimal controller design problem for a seven-segment system. We assume that the control system block diagram is arranged into the standard $\mathbf{P}$–$\mathbf{K}$ configuration shown Figure 6. Here, $\mathbf{w}$ represent the exogenous signals, $\mathbf{z}$ represent the signals of interest, $\mathbf{y}$ represent the measured outputs, and $\mathbf{u}$ represent the control signals. The $\mathbf{P}$ block contains all the uncontrolled dynamics, which include the system dynamics, actuator dynamics, and various pre-designed filters. The $\mathbf{K}$ block contains the controller to be designed.[11]

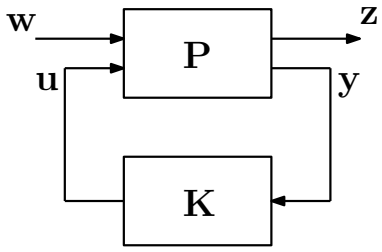

Figure 6. Standard control block diagram configuration

A. Optimal $\mathcal{H}_2$ Control Theory

Lemma 1 *The problem of finding a state-feedback control law that minimizes the linear quadratic objective subject to the dynamics of a linear time-invariant system, i.e.*

$$\begin{aligned} \text{minimize} \quad & J = \int_0^\infty \begin{bmatrix} \mathbf{x}^\mathsf{T}(t) & \mathbf{u}^\mathsf{T}(t) \end{bmatrix} \begin{bmatrix} \mathbf{Q} & \mathbf{S} \\ \mathbf{S}^\mathsf{T} & \mathbf{R} \end{bmatrix} \begin{bmatrix} \mathbf{x}(t) \\ \mathbf{u}(t) \end{bmatrix} dt \\ \text{subject to} \quad & \dot{\mathbf{x}} = \mathbf{A}\mathbf{x} + \mathbf{B}_2\mathbf{u}, \quad \mathbf{u} \in \mathcal{L}_2, \end{aligned}$$

where $\mathbf{Q} = \mathbf{Q}^\mathsf{T} \succeq 0$, $\mathbf{R} = \mathbf{R}^\mathsf{T} \succ 0$, *and* $\begin{bmatrix} \mathbf{Q} & \mathbf{S} \\ \mathbf{S}^\mathsf{T} & \mathbf{R} \end{bmatrix} \succeq 0$ *is equivalent to the optimization problem, defined as*

$$\begin{aligned} \text{minimize} \quad & J = \|\mathbf{z}\|_2^2 = \|\mathbf{C}_1\mathbf{x} + \mathbf{D}_{12}\mathbf{u}\|_2^2 \\ \text{subject to} \quad & \dot{\mathbf{x}} = \mathbf{A}\mathbf{x} + \mathbf{B}_2\mathbf{u}, \quad \mathbf{u} \in \mathcal{L}_2, \end{aligned} \tag{4}$$

where $\mathbf{Q} = \mathbf{C}_1^\mathsf{T}\mathbf{C}_1$, $\mathbf{R} = \mathbf{D}_{12}^\mathsf{T}\mathbf{D}_{12}$, $\mathbf{S} = \mathbf{C}_1^\mathsf{T}\mathbf{D}_{12}$, *and* $\mathbf{z}$ *is the signal of interest whose* $\mathcal{H}_2$*-norm is to be minimized.*

Theorem 1 *Given a plant in the general feedback formulation shown in Figure 6, with*

$$\begin{aligned} \dot{\mathbf{x}} &= \mathbf{A}\mathbf{x} + \mathbf{B}_1\mathbf{w} + \mathbf{B}_2\mathbf{u} \\ \mathbf{z} &= \mathbf{C}_1\mathbf{x} + \mathbf{D}_{12}\mathbf{u} \\ \mathbf{y} &= \mathbf{C}_2\mathbf{x} + \mathbf{D}_{21}\mathbf{w}, \end{aligned}$$

where $\mathbf{x} \in \mathbb{R}^n$, $\mathbf{w} \in \mathbb{R}^{n_w}$, $\mathbf{u} \in \mathbb{R}^{n_u}$, $\mathbf{y} \in \mathbb{R}^{n_y}$ *are the plant states, exogenous inputs, control inputs, and plant outputs, respectively. Assume that* $(\mathbf{A}, \mathbf{B}_2)$ *is stabilizable,* $(\mathbf{A}, \mathbf{C}_1)$ *is detectable, and* $(\mathbf{A}, \mathbf{C}_2)$ *is detectable. Define the Hamiltonian matrices*

$$\mathbf{H}_2 = \begin{bmatrix} \mathbf{A} - \mathbf{B}_2\mathbf{D}_{12}^\mathsf{T}\mathbf{C}_1 & -\mathbf{B}_2\mathbf{B}_2^\mathsf{T} \\ -\mathbf{C}_1^\mathsf{T}\mathbf{C}_1 & -(\mathbf{A} - \mathbf{B}_2\mathbf{D}_{12}^\mathsf{T}\mathbf{C}_1)^\mathsf{T} \end{bmatrix}$$

$$\mathbf{J}_2 = \begin{bmatrix} \mathbf{A}^\mathsf{T} - \mathbf{C}_2^\mathsf{T}\mathbf{D}_{21}\mathbf{B}_1^\mathsf{T} & -\mathbf{C}_2^\mathsf{T}\mathbf{C}_2 \\ -\mathbf{B}_1\mathbf{B}_1^\mathsf{T} & -(\mathbf{A}^\mathsf{T} - \mathbf{C}_2^\mathsf{T}\mathbf{D}_{12}\mathbf{B}_1)^\mathsf{T} \end{bmatrix}.$$

Define the Riccati equation solutions associated with the Hamiltonian matrices $\mathbf{H}_2$ *and* $\mathbf{J}_2$ *by* $\mathbf{X}_R = \mathrm{Ric}(\mathbf{H}_2)$ *and* $\mathbf{Y}_R = \mathrm{Ric}(\mathbf{J}_2)$*, respectively. Define the controller gain and observer gains respectively as*

$$\mathbf{F}_2 = -\left[\mathbf{B}_2^\mathsf{T}\mathbf{X}_R + \mathbf{D}_{12}^\mathsf{T}\mathbf{C}_1\right], \quad \mathbf{L}_2 = -\left[\mathbf{Y}_R\mathbf{C}_2^\mathsf{T} + \mathbf{B}_1\mathbf{D}_{21}^\mathsf{T}\right].$$

Then, the $\mathcal{H}_2$ *optimal controller* $\mathbf{K}(s)$ *to problem (4) has a state-space realization given by*

$$\mathbf{K}(s) \sim \left[\begin{array}{c|c} \mathbf{A} + \mathbf{B}_2\mathbf{F}_2 + \mathbf{L}_2\mathbf{C}_2 & -\mathbf{L}_2 \\ \hline \mathbf{F}_2 & \mathbf{0} \end{array}\right].$$

Moreover, the controller $\mathbf{K}(s)$ *minimizes the* $\mathcal{H}_2$ *norm of the transfer function between the exogenous inputs* $\mathbf{w}$ *and signals of interest* $\mathbf{z}$*,* $\|\mathbf{F}_{zw}\|_2^2$*.*

B. Optimal $\mathcal{H}_2$ problem formulation

The state-space model for a seven-segment system was expressed in Equations (1) and (3). Since we are assuming that we are measuring the direct (absolute) displacements, but the primary objective is to regulate the relative displacements between adjacent segments to zero, we define the variable of primary interest, $\mathbf{z}_1$, as

$$\mathbf{z}_1 = \mathbf{C}_{z_1}\mathbf{x},$$

where $\mathbf{C}_{z_1} \in \mathbb{R}^{6\times 6}$ is the mapping matrix from the state vector $\mathbf{x}$ that describes the displacements and velocities of the supporting points to the relative displacements between adjacent segments. The mapping matrix $\mathbf{C}_{z_1}$ can be readily determined from the geometry of the segmented mirror system and has the structure

$$\mathbf{C}_{z_1} = \begin{bmatrix} \mathbf{C}_{z_1,1} & \mathbf{0}_{6\times 3} \end{bmatrix}.$$

The block diagram that describes the control system for our particular system is shown in Figure 7. The control problem objective is to align seven segments to form a smooth larger segment with minimal efforts.

To formulate the augmented plant shown in Figure 7 into the standard $\mathbf{P}-\mathbf{K}$ block diagram formulation illustrated in Figure 6, we define the exogenous signals and signal of interest respectively as $\tilde{\mathbf{w}} \triangleq \mathbf{w}_0$ and

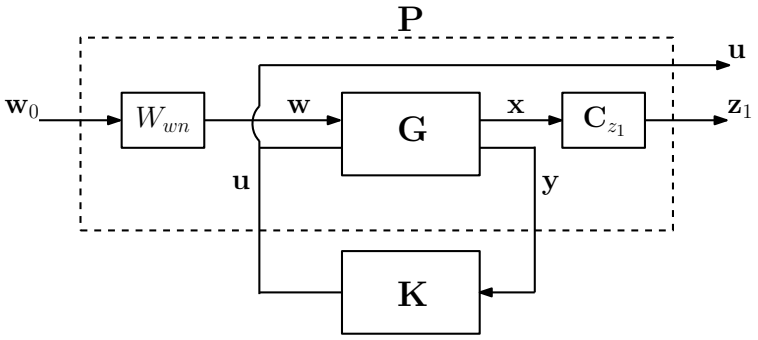

Figure 7. Block diagram of system with augmented plant

$\tilde{\mathbf{z}} \triangleq \begin{bmatrix} \mathbf{z}_1^{\mathsf{T}} & \mathbf{u}^{\mathsf{T}} \end{bmatrix}^{\mathsf{T}}$.

Consequently, the dynamics of the resulting control system block diagram depicted in Figure 6 is given by

$$\dot{\boldsymbol{\chi}} = \tilde{\mathbf{A}}\,\boldsymbol{\chi} + \tilde{\mathbf{B}}_1\,\tilde{\mathbf{w}} + \tilde{\mathbf{B}}_2\,\mathbf{u}, \;\; \tilde{\mathbf{z}} = \tilde{\mathbf{C}}_1\,\boldsymbol{\chi} + \tilde{\mathbf{D}}_{12}\,\mathbf{u}, \;\; \mathbf{y} = \mathbf{C}_2\,\boldsymbol{\chi},$$

where $\boldsymbol{\chi} \triangleq [\mathbf{x}^{\mathsf{T}} \;\; \boldsymbol{\xi}^{\mathsf{T}}]^{\mathsf{T}} \in \mathbb{R}^{84}$, $\tilde{\mathbf{w}} \in \mathbb{R}^{21}$, $\mathbf{u} \in \mathbb{R}^{21}$, $\tilde{\mathbf{z}} \in \mathbb{R}^{84}$, and $\mathbf{y} \in \mathbb{R}^{21}$, and the system matrices are given by

$$\tilde{\mathbf{A}} = \begin{bmatrix} \mathbf{A} & \mathbf{B}_1\mathbf{C}_{\boldsymbol{\xi}} \\ \mathbf{0} & \mathbf{A}_{\boldsymbol{\xi}} \end{bmatrix}, \; \tilde{\mathbf{B}}_1 = \begin{bmatrix} \mathbf{0} \\ \mathbf{B}_{\boldsymbol{\xi}} \end{bmatrix}, \; \tilde{\mathbf{B}}_2 = \begin{bmatrix} \mathbf{B}_2 \\ \mathbf{0} \end{bmatrix}, \; \mathbf{C}_2 = \begin{bmatrix} \mathbf{C} & \mathbf{0} \end{bmatrix}$$

$$\tilde{\mathbf{C}}_1 = \begin{bmatrix} \bar{\mathbf{C}}_1\bar{\mathbf{C}}_{z_1} & \mathbf{0} \end{bmatrix}, \; \bar{\mathbf{C}}_1 = \begin{bmatrix} \bar{\bar{\mathbf{C}}}_1 \\ \mathbf{0} \end{bmatrix}, \; \tilde{\mathbf{D}}_{12} = \begin{bmatrix} \bar{\mathbf{D}}_{12} \\ \mathbf{0} \end{bmatrix},$$

$\bar{\mathbf{C}}_{z_1} = \mathrm{diag}[\mathbf{C}_{z_1}, \ldots, \mathbf{C}_{z_1}]$, where in the formulation above the LQR "tuning" matrices are $\bar{\bar{\mathbf{C}}}_1 = \bar{\bar{\mathbf{C}}}_1^{\mathsf{T}} \succeq 0$ and $\bar{\bar{\mathbf{C}}}_1 \in \mathbb{R}^{42\times 42}$; $\bar{\mathbf{D}}_{12} = \bar{\mathbf{D}}_{12}^{\mathsf{T}} \succ 0$ and $\bar{\mathbf{D}}_{12} \in \mathbb{R}^{21\times 21}$.

IV. Optimal $\mathcal{H}_\infty$ Controller Design for a Seven-Segment System

This section formulates the $\mathcal{H}_\infty$ optimal controller design problem for a seven-segment system. As in Section III, we assume the standard $\mathbf{P}-\mathbf{K}$ block diagram configuration.

A. Optimal $\mathcal{H}_\infty$ Control Theory

It is known that the solution to the $\mathcal{H}_\infty$ controller design problem is not unique.[12] There are several ways to derive an $\mathcal{H}_\infty$ controller. One approach is through a Youla parametrization of the closed loop. However, this often leads to a very high-order controller. Another approach is through an optimization-based reformulation of the Riccati equation that uses linear matrix inequalities. A third approach is through a Riccati-based approach that solves two Riccati equations to find the sub-optimal controller. While the third approach requires several simplifying assumptions, we will adopt this approach as these assumptions are readily satisfied in our formulation.[11]

Theorem 2 *Given a plant in the general feedback formulation shown in Figure 6, with*

$$\begin{aligned} \dot{\mathbf{x}} &= \mathbf{A}\mathbf{x} + \mathbf{B}_1\mathbf{w} + \mathbf{B}_2\mathbf{u}, \; \mathbf{z} = \mathbf{C}_1\mathbf{x} + \mathbf{D}_{11}\mathbf{w} + \mathbf{D}_{12}\mathbf{u} \\ \mathbf{y} &= \mathbf{C}_2\mathbf{x} + \mathbf{D}_{21}\mathbf{w} + \mathbf{D}_{22}\mathbf{u}, \end{aligned}$$

where $\mathbf{x} \in \mathbb{R}^n$, $\mathbf{w} \in \mathbb{R}^{n_w}$, $\mathbf{u} \in \mathbb{R}^{n_u}$, $\mathbf{y} \in \mathbb{R}^{n_y}$ are the plant states, exogenous inputs, control inputs, and plant outputs, respectively. Assume that $(\mathbf{A}, \mathbf{B}_2)$ is stabilizable, $(\mathbf{A}, \mathbf{C}_1)$ is detectable, $(\mathbf{A}, \mathbf{C}_2)$ is detectable, $\mathbf{D}_{11} = \mathbf{0}$, $\mathbf{D}_{22} = \mathbf{0}$, $\mathbf{D}_{12}^{\mathsf{T}}\mathbf{C}_1 = \mathbf{0}$, $\mathbf{D}_{12}^{\mathsf{T}}\mathbf{D}_{12} = \mathbf{I}$, $\mathbf{B}_1\mathbf{D}_{21}^{\mathsf{T}} = \mathbf{0}$, and $\mathbf{D}_{21}\mathbf{D}_{21}^{\mathsf{T}} = \mathbf{I}$. Given $\gamma \in \mathbb{R}_{++}$. Then, there exists an admissible controller with $||\mathbf{F}_{zw}||_\infty < \gamma$ if and only if

- $\mathbf{X}_\infty = \mathrm{Ric}(\mathbf{H}_\infty) \succeq 0$ *for*

$$\mathbf{H}_\infty = \begin{bmatrix} \mathbf{A} & \gamma^{-2}\mathbf{B}_1\mathbf{B}_1^\mathsf{T} - \mathbf{B}_2\mathbf{B}_2^\mathsf{T} \\ -\mathbf{C}_1^\mathsf{T}\mathbf{C}_1 & -\mathbf{A}^\mathsf{T} \end{bmatrix}.$$

- $\mathbf{Y}_\infty = \mathrm{Ric}(\mathbf{J}_\infty) \succeq 0$ *for*

$$\mathbf{J}_\infty = \begin{bmatrix} \mathbf{A}^\mathsf{T} & \gamma^{-2}\mathbf{C}_1^\mathsf{T}\mathbf{C}_1 - \mathbf{C}_2^\mathsf{T}\mathbf{C}_2 \\ -\mathbf{B}_1\mathbf{B}_1^\mathsf{T} & -\mathbf{A} \end{bmatrix}.$$

- $\rho(\mathbf{X}_\infty\mathbf{Y}_\infty) < \gamma^2$.

Further, if the above hold, then the $\mathcal{H}_\infty$ optimal controller $\mathbf{K}(s)$ has a state-space realization given by

$$\mathbf{K}(s) \sim \left[\begin{array}{c|c} \hat{\mathbf{A}}_\infty & -\mathbf{Z}_\infty\mathbf{L}_\infty \\ \hline \mathbf{F}_\infty & \mathbf{0} \end{array}\right],$$

$$\hat{\mathbf{A}}_\infty = \mathbf{A} + \gamma^{-2}\mathbf{B}_1\mathbf{B}_1^\mathsf{T}\mathbf{X}_\infty + \mathbf{B}_2\mathbf{F}_\infty + \mathbf{Z}_\infty\mathbf{L}_\infty\mathbf{C}_2$$
$$\mathbf{F}_\infty = -\mathbf{B}_2^\mathsf{T}\mathbf{X}_\infty,\ \mathbf{L}_\infty = -\mathbf{Y}_\infty\mathbf{C}_2^\mathsf{T},\ \mathbf{Z}_\infty = \left[\mathbf{I} - \gamma^{-2}\mathbf{Y}_\infty\mathbf{X}_\infty\right]^{-1}.$$

B. Optimal $\mathcal{H}_\infty$ problem formulation

Due to the system setup assumed in Theorem 2, we will consider the augmented plant shown in Figure 8. Consequently, we will formulate this augmented plant into the standard $\mathbf{P}-\mathbf{K}$ configuration in Figure 6. For formulation purposes, we will assume that there is an additive sensor noise $\mathbf{v}_0$ and we will design the $\mathcal{H}_\infty$ controller accordingly. However, when simulating the closed-loop system, we will "turn off" such sensor noise for meaningful comparison against the $\mathcal{H}_2$ design.

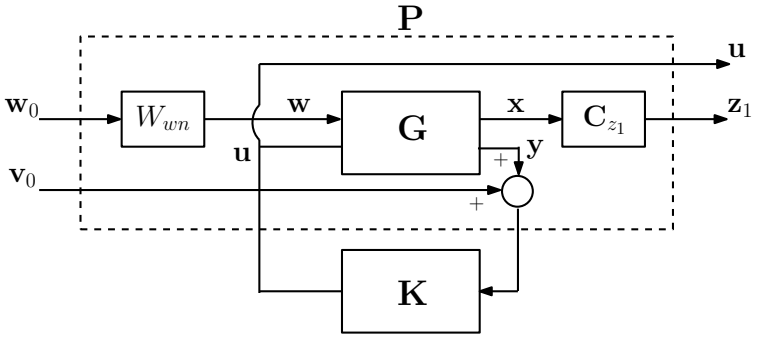

Figure 8. Block diagram of system with augmented plant

To this end, we define the exogenous signals and signal of interest respectively as $\tilde{\mathbf{w}} \triangleq \begin{bmatrix} \mathbf{w}_0^\mathsf{T} & \mathbf{v}_0^\mathsf{T} \end{bmatrix}^\mathsf{T}$ and $\tilde{\mathbf{z}} \triangleq \begin{bmatrix} \mathbf{z}_1^\mathsf{T} & \mathbf{u}^\mathsf{T} \end{bmatrix}^\mathsf{T}$. Hence, the dynamics of the resulting control system is

$$\dot{\boldsymbol{\chi}} = \tilde{\mathbf{A}}\boldsymbol{\chi} + \tilde{\mathbf{B}}_1\tilde{\mathbf{w}} + \tilde{\mathbf{B}}_2\mathbf{u},\ \ \tilde{\mathbf{z}} = \tilde{\mathbf{C}}_1\boldsymbol{\chi} + \tilde{\mathbf{D}}_{12}\,\mathbf{u},\ \ \mathbf{y} = \mathbf{C}_2\boldsymbol{\chi} + \mathbf{D}_{21}\mathbf{w},$$

where $\boldsymbol{\chi} \triangleq [\mathbf{x}^\mathsf{T}\ \ \boldsymbol{\xi}^\mathsf{T}]^\mathsf{T} \in \mathbb{R}^{84}$, $\tilde{\mathbf{w}} \in \mathbb{R}^{42}$, $\mathbf{u} \in \mathbb{R}^{21}$, $\tilde{\mathbf{z}} \in \mathbb{R}^{84}$, $\mathbf{y} \in \mathbb{R}^{21}$, and the system matrices are $\mathbf{D}_{21} = \begin{bmatrix} \mathbf{0} & \mathbf{I} \end{bmatrix}$,

$$\tilde{\mathbf{A}} = \begin{bmatrix} \mathbf{A} & \mathbf{B}_1\mathbf{C}_{\boldsymbol{\xi}} \\ \mathbf{0} & \mathbf{A}_{\boldsymbol{\xi}} \end{bmatrix},\ \tilde{\mathbf{B}}_1 = \begin{bmatrix} \mathbf{0} & \mathbf{0} \\ \mathbf{B}_{\boldsymbol{\xi}} & \mathbf{0} \end{bmatrix},\ \tilde{\mathbf{B}}_2 = \begin{bmatrix} \mathbf{B}_2 \\ \mathbf{0} \end{bmatrix},\ \mathbf{C}_2 = \begin{bmatrix} \mathbf{C} & \mathbf{0} \end{bmatrix}$$
$$\tilde{\mathbf{C}}_1 = \begin{bmatrix} \bar{\mathbf{C}}_{z_1} & \mathbf{0} \end{bmatrix},\ \bar{\mathbf{C}}_{z_1} = \mathrm{diag}[\mathbf{C}_{z_1} \ldots \mathbf{C}_{z_1}],\ \tilde{\mathbf{D}}_{12} = \begin{bmatrix} \mathbf{0} \\ \mathbf{I} \end{bmatrix}.$$

V. Simulations and Results

This section presents open-loop plant analysis and closed-loop system simulations with the designed $\mathcal{H}_2$ and $\mathcal{H}_\infty$ controllers to achieve stabilization of the mirror segments in the presence of wind disturbances. The objective of the control system is to keep the relative displacements between the segments to within 0.1 μm in accordance with the imaging performance requirement (see Section II.F).

A. Open-Loop Plant Analysis

The seven-segment mirror system was constructed and its poles, zeros, and stability were investigated. The system was found to be stable, strictly proper, with no zeros, and with 42 poles. Then, the system was simulated in open-loop configuration, where the initial condition for the positions of the 3 supporting points of each segments were set to be 1 μm. Figure 9 shows the relative displacements between segments 0 and 1. It is clear that the desired imaging performance is not achievable. Similar observations were made for other mirror segments.

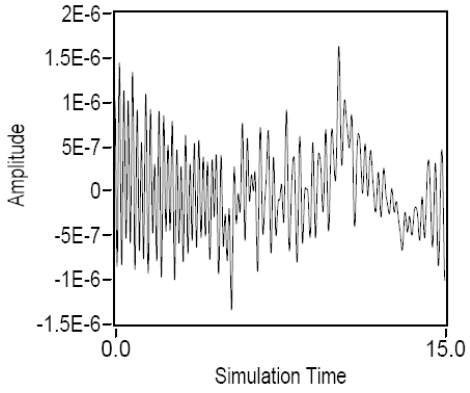

Figure 9. Relative displacement without control

B. Optimal $\mathcal{H}_2$ and $\mathcal{H}_\infty$ Control Simulations

The LQR tuning matrices for $\mathcal{H}_2$ control were set to $\bar{\bar{\mathbf{C}}}_1 = \alpha\,\mathbf{I}_{42\times 42}$ and $\bar{\mathbf{D}}_{12} = \beta\,\mathbf{I}_{21\times 21}$, where $\alpha \in \mathbb{R}_+$ and $\beta \in \mathbb{R}_{++}$ are the tuning parameters. The tuning parameters α and β were set to 1 and 5×10^{-4}, respectively.

In designing the $\mathcal{H}_\infty$ controller, we iterated on the parameter γ starting from the initial iterate $\gamma^{(0)} = 1$ and used the bisection update rule with terminating criterion being the violation of any of the necessary and sufficient conditions for existence of an admissible controller. The corresponding γ was found to be $\gamma = 0.0078$.

Figure 10(a) and 10(b) show the relative displacement between segments 0 and 1 for the $\mathcal{H}_2$ and $\mathcal{H}_\infty$ closed-loop control system, respectively. It is clear that the desired imaging performance was achieved with the designed controllers. It is noted that $\mathcal{H}_2$ achieved slightly better results. This issue can be addressed by introducing appropriate "weighting" filters and consequently adjusting the signal of interest $\mathbf{z}$ so that both controllers perform comparably. Similar observations were made for other mirror segments.

VI. Conclusion and Future Work

This paper derived optimal control laws for a segmented telescope system, where optimality was defined in the $\mathcal{H}_2$ and $\mathcal{H}_\infty$ frameworks. The objective of the control system was to align the segments of the telescope to achieve a desired imaging performance, in the presence of wind disturbances. It was noticed that the designed $\mathcal{H}_2$ and $\mathcal{H}_\infty$ optimal controllers achieved the desired specifications, which were not achievable in open-loop.

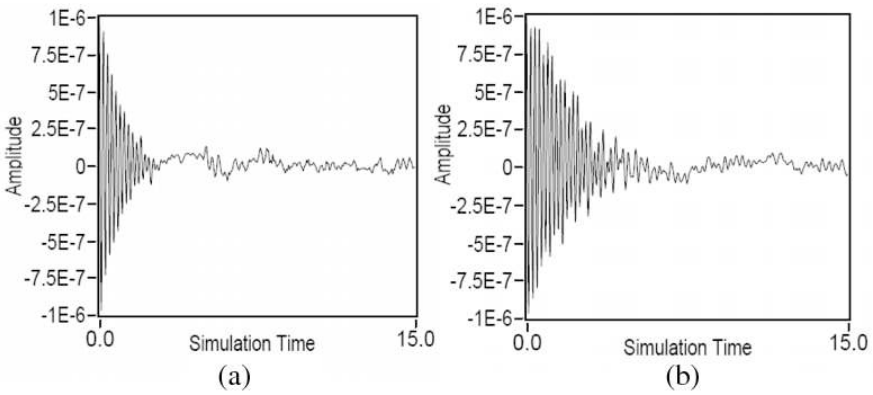

Figure 10. Relative displacement with $\mathcal{H}_2$ and $\mathcal{H}_\infty$ control

Future research is required to make the control system robust to other external disturbances, such as sensor measurement noise, wavefront disturbances, gravity deformations, etc. Moreover, robustness issues with respect to modeling uncertainties and plant parameters mismatches need to be addressed. Finally, fault detection, isolation, and recovery (FDIR) techniques need to be put in place for robust operation against potential system faults.

Appendix

$$\mathbf{A}_i = \begin{bmatrix} \mathbf{0} & \mathbf{I} \\ \mathbf{\Gamma} & \mathbf{\Delta} \end{bmatrix}, \mathbf{\Gamma} = \begin{bmatrix} -625.075 & -180.943 & -180.943 \\ -180.943 & -625.075 & -180.943 \\ -180.943 & -180.943 & -625.075 \end{bmatrix}$$

$$\mathbf{B}_{1,i} = \mathbf{B}_{2,i} = \begin{bmatrix} 0 & 0 & 0 \\ 0 & 0 & 0 \\ 0 & 0 & 0 \\ 0.2194 & 0.0635 & 0.0635 \\ 0.0635 & 0.2194 & 0.0635 \\ 0.0635 & 0.0635 & 0.2194 \end{bmatrix}$$

$$\mathbf{C}_i = \begin{bmatrix} \mathbf{I}_{3\times 3} & \mathbf{0}_{3\times 3} \end{bmatrix}, \mathbf{\Delta} = \begin{bmatrix} -0.219 & -0.064 & -0.064 \\ -0.064 & -0.219 & -0.064 \\ -0.064 & -0.064 & -0.219 \end{bmatrix}$$

$$\mathbf{C}_{z_1,i} = \begin{bmatrix} 1.6667 & -0.7778 & 0.1111 & 0 & 0 & 0 \\ 1.6667 & 0.1111 & -0.7778 & 0 & 0 & 0 \\ 0.1111 & 1.6667 & -0.7778 & 0 & 0 & 0 \\ -0.7778 & 1.6667 & 0.1111 & 0 & 0 & 0 \\ -0.7778 & 0.1111 & 1.6667 & 0 & 0 & 0 \\ 0.1111 & -0.7778 & 1.6667 & 0 & 0 & 0 \end{bmatrix}.$$

$$\mathbf{A}_{\xi_i} = \begin{bmatrix} -11.04 & -8.36 \\ 1 & 0 \end{bmatrix}, \mathbf{B}_{\xi_i} = \begin{bmatrix} 1 \\ 0 \end{bmatrix}, \mathbf{C}_{\xi_i} = \begin{bmatrix} 1.69 & 26.44 \end{bmatrix}.$$

Acknowledgments

The authors would like to thank Bertrand Bauvir, Lothar Wenzel, and Michael Cerna for their constructive feedback.

References

[1]J. Aubrun, K. Lorell, T. Mast, and J. Nelson, "Dynamic analysis of the actively controlled segmented mirror of the W.M. Keck ten-meter telescope," *IEEE Control Systems Magazine*, vol. 7, no. 6, pp. 3–10, 1987.

[2]D. Silva, P. Hickson, C. Steidel, and M. Bolte, *Thirty Meter Telescope Detailed Science Case*, 2007.

[3]D. MacMartin, "Control challenges for extremely large telescopes," in *Proceedings of SPIE Commercial and Industrial Applications of Smart Structures*, vol. 5054, March 2003, pp. 275–286.

[4]ESO, *E-ELT*, 2010. [Online]. Available: www.eso.org/public/astronomy/projects/e-elt.html

[5]J. Spyromilio, *Developing Real-Time Control for the World's Largest Telescope Using* NI L*ab*VIEW *With Multicore Functionality*, 2010. [Online]. Available: http://sine.ni.com/cs/app/doc/p/id/cs-11465

[6]S. McCaslin, L. Wenzel, J. Meisel, and M. Cerna, "Controlling extremely large telescopes," in *Proceedings of the international conference of high performance computing networking, storage, and analysis*, November 2008.

[7]P. Bely, *The Design and Construction of Large Optical Telescopes*. New York: Springer-Verlag, 2003.

[8]S. Jiang, P. Voulgaris, L. Holloway, and L. Thompson, "H_2 control of large segmented telescopes," *Journal of Vibration and Control*, vol. 15, no. 6, pp. 923–949, 2009.

[9]M. Quattri, F. Koch, L. Noethe, A. Bonnet, and S. Noelting, "OWL wind loading characterization: a preliminary study," in *Proceedings of S.P.I.E.*, vol. 4840, January 2003, pp. 459–470.

[10]G. Angeli, M. Cho, M. Sheehan, , and L. Stepp, "Characterization of wind loading of telescopes," in *Proceedings of SPIE*, February 2002, pp. 72–83.

[11]U. Mackenroth, *Robust Control Systems: Theory and Case Studies*. New York: Springer-Verlag, 2004.

[12]J. Doyle, K. Glover, P. Khargonekar, and B. Francis, "State-space solutions to standard H_2 and H_∞ control problems," *IEEE Transactions on Automatic Control*, vol. 34, no. 8, pp. 831–847, 1989.